J. Phys. D: Appl. Phys. **33** (2000) 101–106. Printed in the UK PII: S0022-3727(00)08131-6

Powerful interface light emitting diodes for methane gas detection

A Krier and V V Sherstnev†

Physics Department, Lancaster University, Lancaster LA1 4YB, UK

Received 24 September 1999

Abstract. Powerful (light emitting diodes) LEDs which exhibit more than 3.5 mW of output power at room temperature have been fabricated by liquid phase epitaxy (LPE) and characterized. These LEDs are well matched to the CH_4 absorption spectrum and confirm the potential of the devices as a key component for use in an infrared CH_4 gas sensor. We report on the efficient interface electroluminescence in our LEDs across the InAs/InAsSbP heterojunction consistent with type II emission. This directly suppresses the Auger recombination and enables these sources to emit maximum powers in excess of 3 mW at room temperature. Furthermore, the use of Yb rare earth ion gettering in these devices was found to be effective in increasing the LED output power. We attribute this to a reduction in the residual carrier concentration arising from the removal of unintentional donors and point defects in the InAs active region material. The ring contact geometry was also found to be superior when compared to the dot contacts in our structures.

The LEDs demonstrated in this work are sufficiently powerful to be used in a practical methane gas sensor.

(Some figures in this article appear in colour in the electronic version; see `www.iop.org`)

1. Introduction

Mid-infrared light emitting diodes (LEDs) have recently been extensively studied [1–3, 12] due to their potential applications in the areas of remote sensing, pollution monitoring and infrared countermeasures. Significant progress has been made in the development of mid-infrared (2–5 μm) LEDs, with much of the recent research in this spectral range focused on interband antimonide devices utilizing a variety of quantum-well and superlattice designs. If they can provide enough output power, then selective, highly sensitive gas sensor instrumentation can be constructed based on such mid-infrared sources of radiation. Currently, pulsed filament sources suffer from inherently slow modulation, whereas incandescent bulbs are limited to <4 μm by the glass envelope of the source and require burning-in before they become stable. From an engineering viewpoint, LEDs do not have these drawbacks and offer the additional advantages of room-temperature operation, simplicity, low electric power consumption, and are likely to be more cost effective than diode lasers for deployment in practical gas sensors. In the present work we report on the fabrication of powerful mid-infrared LEDs operating at room temperature specifically for methane gas detection.

The spectral region around 3.3 μm is attractive for the purpose of detecting C–H in various environments, since it contains the fundamental C–H absorption line [4]. A detailed examination of the methane gas absorption spectrum reveals that there are in fact three principal absorptions, i.e. the P, Q and R branches which are found at the following wavelengths; CH_4, $P = 3.31$ μm, $Q = 3.28$ μm and $R = 3.21$ μm [4], the most intense of these being the absorption line associated with the Q-branch which forms the centre of the absorption spectrum and which is naturally our target wavelength. InAs has a room-temperature energy bandgap of 0.354 eV ($\lambda_g = 3.5$ μm is near the centre wavelength of the CH_4 absorption) and so is a good choice as a starting-point material for the fabrication of LEDs for methane detection. However, there are difficulties associated with the following; arsenic vacancies (V_{As}) which produce donor levels 0.1–0.2 eV below the conduction band, residual impurities (e.g. S, Se, Te) which result in 10–20 meV shallow donors, as well as unknown acceptor states with ionization energy of 50 meV [5, 6]. It is possible to overcome the problem of arsenic vacancies by liquid phase epitaxy (LPE) growth at temperatures above 600 °C, but this still leaves residual impurities. More recent efforts have centred around using low concentrations of rare earth elements which are deliberately added to the growth solutions to act as effective gettering agents. The results have already shown that the common impurities (for example S, Se, Si, C, Te, O, etc) can readily form stable compounds with reactive rare earth elements such as Gd, Yb and Er. These compounds are insoluble in indium (which is the most common solvent used in LPE growth of InAs based alloys) [5] and so are not incorporated at all into the grown solid epitaxial layer. Therefore, rare earth gettering is an attractive means

† EPSRC visiting research fellow from Ioffe Institute, St Petersburg, Russia.

Table 1. Comparison of residual carrier concentrations obtained by using rare earth gettering to purify epitaxial InAs grown by LPE.

Rare earth element used	Amount of rare earth gettering agent added to melt (at%)	Residual carrier concentration (cm^{-3})	Temperature (K)	Reference
Gd	1.84×10^{-6}	9×10^{15}	300	[2, 3]
Gd	5.1×10^{-6}	1.3×10^{16}	77	[4]
Yb	3×10^{-6}	$<5 \times 10^{15}$	300	[5]

of removing unwanted impurities from LPE grown InAs solid solutions and reducing the background doping level towards 10^{15} cm^{-3} [5–8]. Some results are summarized in table 1.

In this paper we report significant improvements in the output power of InAs LEDs to above 3 mW at room temperature. This was achieved using three techniques; type II interface structures for Auger suppression, rare-earth gettering for reduction of Shockley–Read–Hall recombination and ring contact geometry to improve current spreading.

2. Experimental procedures

The LEDs were fabricated from double heterostructures (DHs) (see figure 1) grown by LPE. A conventional horizontal, multi-well graphite sliding boat was used for the LPE growth of the LED structures. Epitaxy was carried out with the boat inside a high-purity quartz reactor tube under flowing purified hydrogen gas from a Pd-diffusion unit. The apparatus was fully automated and controlled with *Labview* operating software from a PC. The resulting epitaxial structure was a DH in which the unintentionally doped n-InAs active layer is enclosed between p– and n–InAsSbP confinement layers. The P content in the confinement layers is 0.40 (E_g = 570 meV, T = 300 K) to provide a higher bandgap energy and large interface band offsets for good carrier confinement. The InAs active region was 0.7 μm thick (E_g = 354 meV, T = 300 K), and the InAsSbP layers were iso-periodic with InAs and each 3.0 μm in thickness. The InAs/InAsSbP heterostructure is type II in nature and although the structure contains no quantum wells, the band bending at the interface leads to some confinement of electrons and holes on opposite sides (see figure 7 later), which affords the possibility of reduced Auger recombination and increased electroluminescence at room temperature.

By using Yb rare earth gettering the residual carrier concentration in the active layer was reduced to less than 5×10^{15} cm^{-3} (T = 300 K—see below), the cladding layers were doped with Sn up to a concentration of 5×10^{18} cm^{-3} and with Zn up to 1×10^{18} cm^{-3} for N and P sides, respectively. The epitaxial structures were grown onto (100) oriented p-type InAs substrates obtained from Wafer Technology Ltd.

In order to investigate the effect of material purity on the quantum efficiency of the active region, two different types of devices were fabricated in which the same epitaxial growth procedure was used for each, but the nature of the source material was different. The different precursors used were as follows: monocrystal InAs + Yb (used for LED I) and monocrystal InAs (used for LED II). The purpose of the

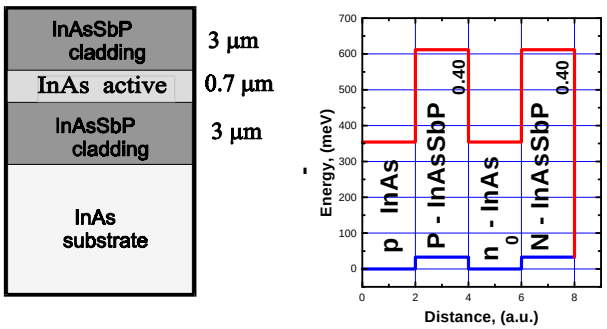

Figure 1. The basic device structure and the energy-band diagram of the InAsSbP/InAs/InAsSbP double heterostructure LEDs grown by LPE.

Yb was to act as a gettering agent in the growth solution in order to remove impurities (S, Si etc), and to further improve the quantum efficiency of the layer. Two different types of LED chips were produced for comparison. For the first type (LED I) square chips of dimensions of a 450×450 μm^2 (emitting area 2×10^{-3} cm^2) were defined and etched-out without forming a mesa structure. Only LEDs of type I were prepared with the benefit of Yb gettering of the LPE growth melt as described above. For the second type (LED II) mesa diodes were fabricated from the epitaxial wafers by conventional photolithography and wet chemical etching to produce mesas† 300 μm in diameter (emitting area 7×10^{-4} cm^2). Ohmic contacts were formed by thermal evaporation of Au:Zn and Au:Te on the p- and n-sides of the wafers, respectively, at 180 °C and the LED chips were, using a small amount of In solder, then mounted onto TO49 headers for testing. A 300 μm diameter ring contact was deposited for the square diodes (LED I), whereas a 40 μm diameter dot-contact pad was used for the mesa diodes (LED II). A Nomarski microscope photograph of each of the two types of LEDs is shown in figure 2. In each case the radiation is extracted through the upper cladding layer. Once the LED chips were assembled in this manner onto standard TO49 packages ready for testing, they were equipped with a small home-made parabolic reflector in order to help collimate all of the LED output. The full-width at half-maximum (FWHM) of the resulting output beam obtained with this arrangement (for each LED type) was about 12°. Since the LED chip was effectively placed at the focus of a parabola, the output beam was focused to a small spot (<1 mm) at a distance about 40 mm away, which is near optimal for many gas sensor instrument applications.

Current–voltage (I–V) measurements were made using an automatic system, based on a high performance op-amp

† The LEDs were defined by chemically etching a small raised area or mesa into epitaxial layers.

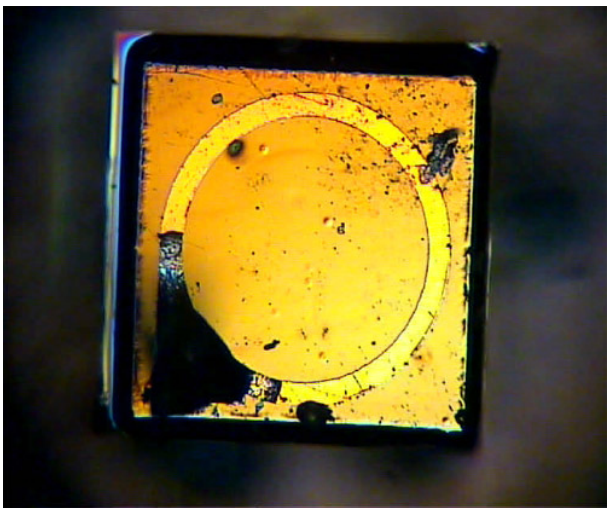

(*a*)

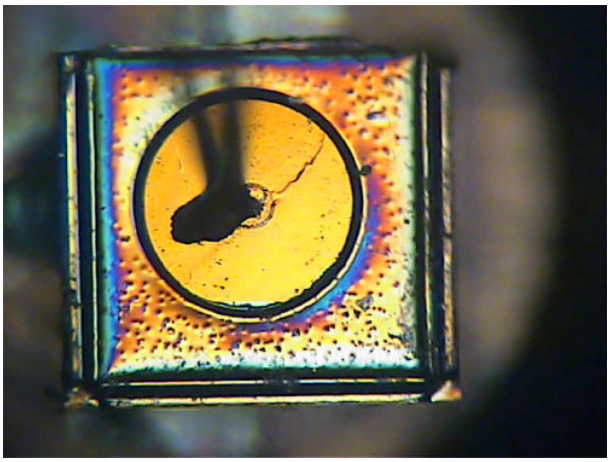

(*b*)

Figure 2. Nomarski microscope photographs of: (a) LED I, which is a 450 × 450 μm^2 square (emitting area 2.0 × 10^{-3} cm^2) with a ring contact 300 μm in diameter, and (b) LED II, a mesa-etched LED chip with a diameter of 300 μm (emitting area 7 × 10^{-4} cm^2).

IC LM759 which features high-output-current capability, and is designed to operate from a single or dual power supply with an input common mode range that includes the negative supply. The data was read by a GPIB (general purpose interface bus) interface card that was connected to a voltage calibrator, voltmeter and ammeter, and was plotted automatically.

The electroluminescence emission spectra from the LEDs and light–current characteristics were typically measured at 300 K using 2 μS current pulses of up to 2 A (at a duty cycle of 0.2%) and a frequency of 1 kHz. After passing through the cryostat windows the radiation was collected using CaF_2 lenses and focused into a 1 m Monospek 1000 monochromator. The electroluminescence was detected using a cooled (77 K) InSb photodiode detector and Stanford Research (SR850) digital phase-sensitive detector. A PC was used to control the monochromator and record the final signal using *Labview* operating software.

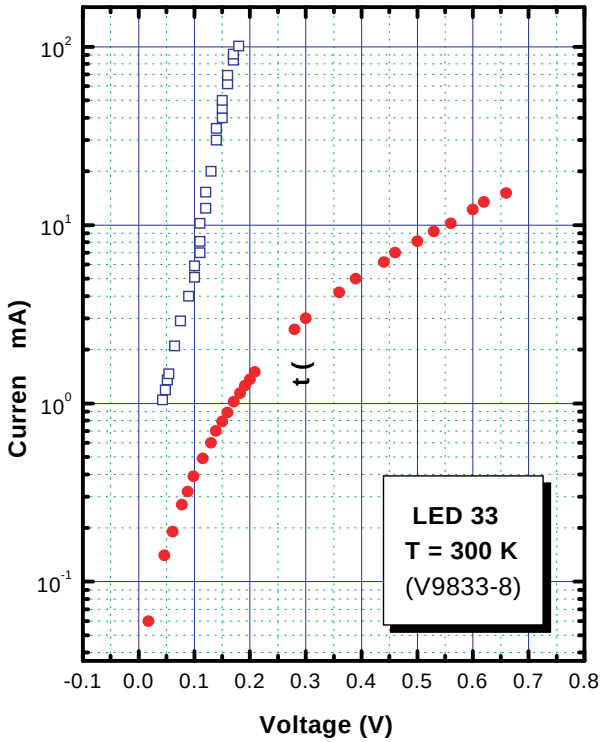

Figure 3. A semi-logarithmic plot of a typical current–voltage characteristic for one of the square LED chips (LED I) measured at room temperature.

3. Results

The current–voltage characteristic obtained from LED I is shown in the semi-logarithmic plot of figure 3 and indicates that this LED had a good diode character with a turn-on voltage of ∼0.06 V at room temperature. The inflection in the I–V characteristic at small current corresponds to some slight crowding of the current in the junction area just below the contact. For small carrier concentrations in semiconductor p–n heterojunctions, recombination and generation take place to an appreciable extent in the barrier region itself. As a result, the effectiveness of the barrier in differentiating the two currents is reduced, and a modified form of the current equation is often used to describe the I–V characteristic of a real diode. This is

$$I \cong I_0 \left[\exp\left(\frac{eV}{\eta kT} \right) - 1 \right]$$

where e is the electric charge, V is the applied voltage, k is Boltzmann's constant, T is the temperature, $I_0 \sim 0.6$ mA is the saturation current and η is the ideality factor, which we determined from figure 3 to be $\eta = 3.5$. The combined junction and contact resistance of the diode was found to be ∼0.5 Ω.

The diodes can operate both quasi-continuously (50% duty cycle) and in pulsed mode at room temperature. The quasi-continuous electroluminescence emission spectrum of a typical type I LED at room temperature is shown in figure 4. A single peak is obtained at 3.28 μm, which is almost the same as the bandgap energy of the active region, and

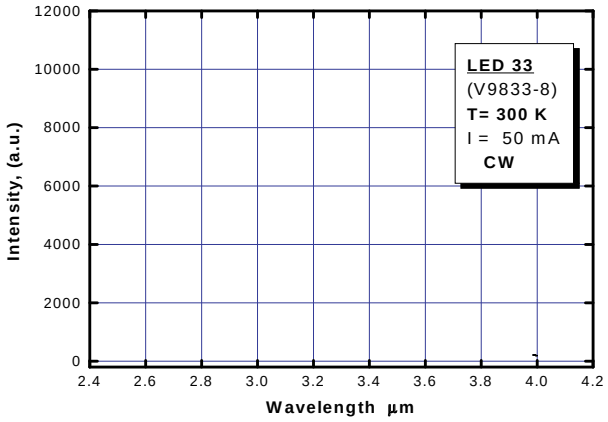

Figure 4. The room-temperature electroluminescence emission spectrum obtained from one of the LEDs (LED I) with a purified active region, measured at a drive current of 50 mA at 430 Hz using a 50% duty cycle.

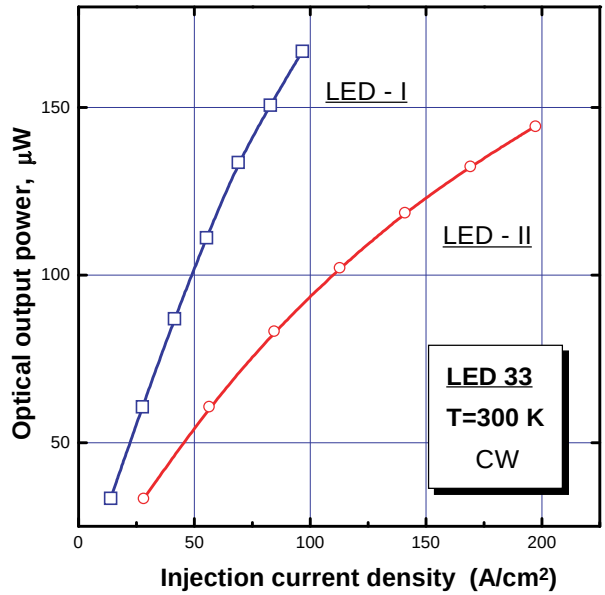

Figure 5. Light–current characteristics measured from the LEDs prepared with different contact geometries. LED I is 450×450 μm^2 square with a ring contact 300 μm in diameter and a Yb purified active region, LED II is a mesa-etched LED chip with a diameter of 300 μm. The characteristics were measured at room temperature using a 50% duty cycle at 430 Hz.

which is exactly coincident with the Q-branch absorption of methane gas. Furthermore, the LEDs peak wavelength remains constant over the whole range of the drive currents used, unlike the situation in bulk InAs homojunction LEDs. The FWHM of the spectrum increases only slightly with drive current and was measured to be 0.5 μm for these 3.28 μm LEDs.

The output power of the two types of InAs-based diodes against pulsed injection current density is presented in figure 5. The absolute power was measured by a calibrated pyroelectric power meter (Laser Precision, RS5710). The curves are linear at low current densities, with the slope decreasing more quickly for LED II than for LED I (which is quite linear up to 90 A cm^{-2}) at high current densities.

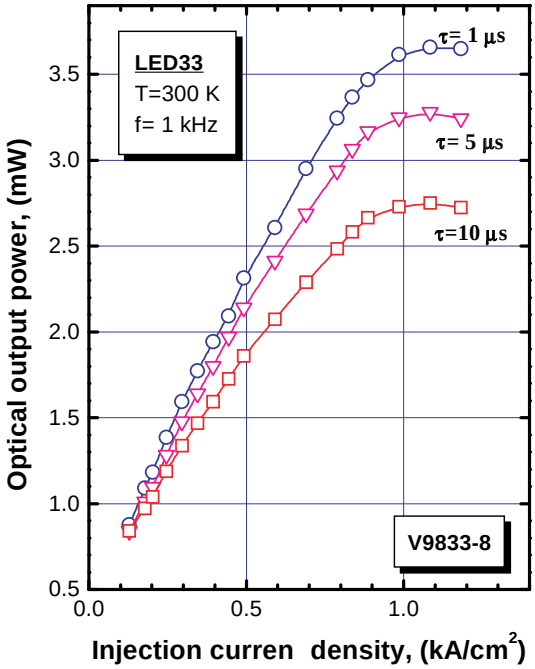

Figure 6. Light–current characteristics measured from LED I. The characteristics were measured at room temperature at a drive current of 1 kHz using 0.1%, 0.5% and 1% duty cycles with 1 μs, 5 μs and 10 μs pulses, respectively.

To find the range of injection currents where overheating effects do not dominate, the optical output power of one 3.28 μm LED was measured at 300 K with different pulse widths at the same repetition rate (1 kHz). The results are shown in figure 6. The pulsed optical power did not depend strongly on the pulse width (τ), which was varied from 1 to 10 μs, and the characteristics were quite linear up to a current density of about 1 kA cm^{-2}. At higher injection currents the slope of the curves decreased with increasing pulse duration. For 5 μs long pulses, (which corresponds to the PbSe detector response speed appropriate for use in gas sensor instrumentation) the output power saturated at a current density of 1 kA cm^{-2} at a value of more than 3 mW. Using the shortest current pulses with τ of 1 μs, a maximum output power in excess of 3.5 mW was readily achieved using a drive current of 2 A (i.e. at a current density of 1 kA cm^{-2}, which is still a low injection level compared with that in diode lasers).

4. Discussion

The emission spectrum of the heterostructure LED measured at room temperature consists of a single emission line (as shown in figure 4). The slight inflection near 2.7 μm is due to water vapour absorption from the atmosphere. The radiative and electrical properties of the LEDs of both types are essentially determined by the InAs/InAsSbP DH active region (and broadened by thermal distribution of carriers). However, the peak wavelength of 3.28 μm is not the same as that expected from the InAs energy gap, i.e. $\lambda_g = 3.50$ μm at 300 K. The emission is also observed to be much more intense (in both LED I and LED II) than in similar epitaxial homojunction InAs LEDs. Such high-power electroluminescence

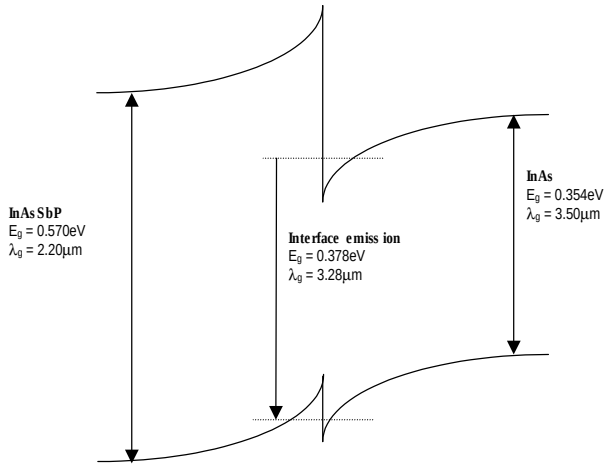

Figure 7. A schematic energy-band diagram of the heterojunction showing the type II interface transition observed in our LEDs at 3.28 μm in the room-temperature electroluminescence spectrum.

emission at higher energy than the bandgap (i.e. 3.28 μm) and in a single line which is insensitive to drive current is entirely consistent with emission which originates from a type II transition at the InAs/InAsSbP heterojunction interface as shown in figure 7.

We can account for the improvements in the output power in our LEDs by simply considering the carrier recombination mechanisms which are operating in the diode. At equilibrium, the total recombination rate R_{tot} per unit area is given by [9]:

$$R_{tot} = e(A_{SRH}n + B_{Rad}n^2 + C_{Auger}n^3)h$$

where n is the carrier density in the active layer, e is the electric charge and h is the thickness of the active layer. The total recombination rate R_{tot} includes band-to-trap non-radiative recombination $A_{SRH}n$, band-to-band radiative recombination $B_{Rad}n^2$ and Auger recombination $C_{Auger}n^3$. The coefficient C has an exponential temperature dependence and takes the following form

$$C_{Auger} = C_0 \exp(-E_a/kT)$$

where $E_a = [m_e/(2m_{hh})]E_g$ with E_a as the activation energy for the Auger process (and m_e and m_{hh} are the respective electron and heavy hole effective masses).

In this work we have increased the total output power by minimizing the non-radiative recombination in two ways. First, because the dominant radiative transition occurs across the interface (see figure 7) and is type II in nature since the electrons and holes are localized on opposite sides of the heterojunction, then Auger recombination is directly suppressed and the coefficient C is reduced in the equation above. Because these levels are localized there is little wavelength shift with increasing drive current and this type II interface recombination mechanism is operative in both types of LEDs. Second, by using Yb ions as gettering agents for the melt purification during LPE growth of the LED active region we have reduced the number of non-radiative recombination centres and so directly reduced the coefficient A. Because reducing the number of such centres and shallow donors also reduces the residual carrier concentration this indirectly reduces the last term $C_{Auger}n^3$. This accounts mainly for the difference in performance between LED I (with Yb) and LED II as shown in figure 5. Previously we observed a factor of two improvement in the output power for InAsSb LEDs by using Yb gettering to purify the active region [10]. This is in good agreement with the improvement obtained here for LEDs with InAs in the active region. The relative importance of the two terms $A_{SRH}n$, and $C_{Auger}n^3$ depends on the temperature and also on the injection level in the device when it is operating. In this respect the $A_{SRH}n$ term is thought to dominate at low temperatures, while the $C_{Auger}n^3$ term dominates at room temperature. This is certainly the case under high injection conditions. However, for our LEDs the injection level is lower (typically $\sim 5 \times 10^{16}$ cm^{-3}) and so Shockley–Read–Hall recombination is also important, which is why we observe an improvement due to the Yb gettering at 300 K.

Finally, we should account for the difference in the two types of LEDs with respect to the different contact geometry and size. Type I LEDs (with Yb) were square with a square emitting area and ring contact, and the type II LEDs comprised a mesa etched emitter with a central dot contact pad (see figure 2). Most of the performance improvement in efficiency we attribute directly to the effect of Yb gettering, but, with reference to figure 5, LED I has a more linear characteristic than LED II and saturation is not so readily apparent. We can attribute this improvement to the better current spreading into the active region achieved with the ring contact. This is consistent with simple geometrical calculations.

5. Conclusions

Powerful LEDs which exhibit more than 3.5 mW of output power at room temperature have been fabricated and characterized. These LEDs are well matched to the CH_4 absorption and confirm the potential of the devices as a key component for use in an infrared CH_4 gas sensor. We correlate the electroluminescence in both types of LEDs used with type II emission across the InAs/InAsSbP heterojunction interface. This has the additional benefit of directly reducing Auger recombination and enables these sources to emit maximum powers in excess of 3 mW at room temperature, which is a significant improvement compared with previous results [11–14]. Furthermore, the effect of Yb rare earth ion gettering in these devices produced an increase in output power of at least a factor of two. We attribute this to a reduction in the residual carrier concentration arising from the removal of unintentional donors and point defects in the active region of the material. Although Auger recombination is thought to be a limitation to the operation of room-temperature mid-infrared sources, our results indicate that the elimination of Shockley–Read–Hall recombination centres is also an important issue. The ring contact geometry was also found to be superior than dot contacts in our structures.

We consider the devices prepared and characterized in this work to be a major step forward towards an LED-based CH_4 gas sensor.

Acknowledgment

We wish to thank EPSRC for the award of a visiting fellowship for V Sherstnev.

References

[1] See for example, Matveev B *et al* 1998 InAsSbP/InAs LEDs for the 3.3–5.5 μm spectral range *IEE Proc. Optoelectron.* **145** (Special Issue on Mid-IR devices and materials and papers therein, see also vol 144 (1997) for additional related papers)

[2] Krier A, Gao H, Sherstnev V and Yakovlev Yu 1999 High Power 4.6 μm LED's for CO detection grown by LPE using rare earth gettering *Electron. Lett.* **35** 1665–7

[3] Baranov A N, Imenkov A N, Kapranchik O P, Negreskul V V, Chernyavskii A G, Sherstnev V V and Yakovlev Yu P 1990 Long-wavelength light-emitting diodes, based on InAsSbP/InAs heterostructures ($\lambda = 3.0$–4.8 μm) at 300 K with wide-gap window *Pisma v Z. Tekh. Fiz.* **16** 42–7

[4] Rothman L S *et al* 1992 The HITRAN molecular database: edition of 1991 and 1992 *J. Quant. Spectrosc. Radiat. Transfer* **48** 469–507

[5] Krier A, Gao H H and Sherstnev V V 1999 Purification of epitaxial InAs grown by liquid phase epitaxy using gadolinium gettering *J. Appl. Phys.* **85** 8419–22

[6] Gao H H, Krier A and Sherstnev V V 1999 High quality InAs grown by liquid phase epitaxy using gadolinium gettering *Semicond. Sci. Technol.* **14** 441–5

[7] Baranov A N, Voronina T I, Logunova T S, Sipovskaya M A, Sherstnev V V and Yakovlev Yu P 1993 Properties of epitaxial indium arsenide doped with rare-earth elements *Semiconductors* **27** 236–40

[8] Zotova N V, Karandashev S A, Matveev B A, Remenny M A, Stus N M and Talalakin G N 1999 Gadolinium-doped InAs-based InGaAsSb solid solutions for light diodes in a spectral region of $\lambda = 3$–5 μm *Semiconductors* **33** 1010–13

[9] Kim S, Erdtmann M, Wu D, Kass E, Yi H, Diaz J and Razeghi M 1996 Photoluminescence study of InAsSb/InAsSbP heterostructures grown by low-pressure metalorganic chemical vapor deposition *Appl. Phys. Lett.* **69** 1614–16

[10] Krier A, Gao H H, Sherstnev V V and Yakovlev Y High power 4.6 μm light emitting diodes for CO detection *J. Phys. D: Appl. Phys.* **32** 3117–21

[11] Parry M K and Krier A 1994 Efficient 3.3 μm light emitting diodes for detecting methane gas at room temperature *Electron. Lett.* **30** 1968–9

[12] Popov A, Sherstnev V, Yakovlev Yu, Baranov A and Alibert C 1997 Powerful mid-infrared emitting diodes for pollution monitoring *Electron. Lett.* **30** 86–8

[13] Popov A A, Stepanov M V, Sherstnev V V and Yakovlev Yu P 1997 3.3 μm LEDs for measurement of methane *Tech. Phys. Lett.* **23** 828–30

[14] Kim S, Erdtmann M, Wu D, Kass W, Yi H, Diaz J and Razeghi M 1999 Photoluminescence study of InAsSb/InAsSbP heterostructures grown by low-pressure metalorganic chemical vapor deposition *Appl. Phys. Lett.* **69** 1614–16